

# Identification of selected sources from the ROSAT Galactic Plane Survey - I <sup>\*</sup>

C. Motch<sup>1</sup>, P. Guillout<sup>2,1</sup>, F. Haberl<sup>2</sup>, J. Krautter<sup>3</sup>, M.W. Pakull<sup>1</sup>, W. Pietsch<sup>2</sup>, K. Reinsch<sup>4</sup>, W. Voges<sup>2</sup>, and F.-J. Zickgraf<sup>1</sup>

<sup>1</sup> Observatoire Astronomique, UA 1280 CNRS, 11 rue de l'Université, F-67000 Strasbourg, France

<sup>2</sup> Max-Planck-Institut für extraterrestrische Physik, D-85740, Garching bei München, Germany

<sup>3</sup> Landessternwarte, D-69117 Heidelberg-Königstuhl, Germany

<sup>4</sup> Universitäts-Sternwarte, Geismarlandstrasse 11, D-37083, Göttingen, Germany

Submitted to Astronomy & Astrophysics, Supplement Series. Received / Accepted

**Abstract.** We report on optical searches in the error circles of 93 ROSAT survey sources located at low galactic latitudes ( $|b| < 20^\circ$ ). These sources were extracted from the ROSAT Galactic Plane Survey using various selection criteria on hardness ratio, X-ray and optical brightness and integrated galactic absorption in the direction of the source. We find optical identifications in 76 cases, among which are 25 new AGN, 6 new CVs and a new Be/X-ray binary. In order to illustrate the relevance of the source selections applied here, we cross-correlated the ROSAT all-sky survey bright source list with SIMBAD. Different classes of X-ray emitters populate distinct regions of a multi dimensional parameter space involving flux ratios, galactic latitude and  $N_{\text{H}}$ . This relatively good segregation offers the possibility to build source samples with enhanced probability of identification with a given class. Complete optical identification of such subsamples could eventually be used to compute meaningful probabilities of identification for all sources using as basis a restricted set of multi-wavelength information.

**Key words:** X-ray general, X-ray stars, stars: activity, stars: neutron, stars: statistics

Sensitive Proportional Counter (PSPC, Pfeffermann et al. 1986). The survey mapped as many as 60,000 new sources in the soft X-ray band (0.1-2.4 keV,  $ML \geq 10$ ) down to limiting fluxes of the order of a few  $10^{-13} \text{ erg cm}^{-2} \text{ s}^{-1}$ . Recently, the 18,811 RASS sources having a PSPC count rate larger than  $0.05 \text{ cts s}^{-1}$  and  $ML \geq 15$  have been published (Voges et al. 1996). The study of the RASS point source content at low galactic latitudes ( $b \leq 20^\circ$ ) is the scope of a dedicated project, the ROSAT Galactic Plane Survey (RGPS: Motch et al. 1991). About 15,000 RASS sources are located in this  $40^\circ$  wide strip of the sky.

In the galactic plane area, already 20% to 30% of RGPS sources may be identified with high confidence on the basis of positional coincidence with objects, mostly stars, catalogued in the SIMBAD database. Adding cross-correlation with relatively bright stellar catalogues such as Guide Star Catalogue entries allows the identification of about 50% of RGPS sources (Motch et al. 1997a).

The number of remaining unidentified sources is however still too large to allow their systematic identification at the telescope. In order to tackle this problem, two paths of investigations were chosen; i) selection of sources over the whole galactic sky using criteria on their X-ray characteristics and optical content of the error box and ii) selection of sample areas at judicious positions for complete optical identification.

The X-ray selected approach has led to the discovery of a number of interesting objects, mostly soft sources which have escaped previous surveys carried out at higher energies and furthermore without imaging instrumentation or large sky coverage. Among the most noticeable results are the discovery of galactic supersoft sources (Ögelman et al., 1993, Motch et al. 1994, Beuermann et al. 1995), a new class of soft intermediate polars (Haberl & Motch 1995), and more recently the identification of a couple of isolated

## 1. Introduction

The ROSAT all-sky survey (RASS; Voges 1992) was performed from 1990 July till 1991 February and was carried out with the X-ray telescope (XRT) and the Position

*Send offprint requests to:* C. Motch

<sup>\*</sup> Partly based on observations obtained at the European Southern Observatory, La Silla (Chile) with the 2.2m telescope of the Max-Planck-Society, with the ESO 1.5m telescope and at the Observatoire de Haute-Provence, CNRS, France

neutron stars presumably accreting from the interstellar medium (Walter et al. 1996, Haberl et al. 1997).

On the other hand, systematic optical identification of RGPS sources in sample areas has led to the conclusion that active coronae dominate by number the point source content (up to 85% of the total; Motch et al. 1997a). In contrast, the stellar fraction identified at high galactic latitude is much lower (12-63%; Zickgraf et al., 1997). The modelling of this stellar population and ages derived from Lithium lines clearly show that the stars detected in the RASS are quite young, mostly younger than 1Gyr (Guillout et al. 1996a,b). Another important result from this study is derived from the small number of sources remaining unidentified. In particular, this implies that the space density of isolated neutron stars accreting from the interstellar medium is at least a factor 10 smaller than expected.

This paper is divided in two parts. First we show how X-ray and optical characteristics of ROSAT sources may be used to build samples with enhanced probabilities of identification with a given class of object. For that purpose we cross-identified the ROSAT all sky survey bright source list with SIMBAD. Second, we report on optical observations of 93 selected RGPS sources. The source list contains various kinds of X-ray selected sub samples out of which several identifications not repeated here were already published.

Our identification programme of X-ray selected sources in the galactic plane is continuing and we expect to provide more RGPS source identifications in a future paper.

## 2. Cross-identification of the ROSAT all-sky survey bright source catalogue with SIMBAD

### 2.1. BRASS-SIMBAD correlation

Studying the clustering properties of identified X-ray sources in a multi-wavelength parameter space can help finding domains in which the probability of association with a given class of object is higher than on the average. For instance, at low galactic latitude the overwhelming domination of stellar coronae makes the discovery of new CV a difficult task as they only account for  $\approx 1\%$  of the total number of sources (Motch et al. 1996) whereas their frequency is much higher among either hard, or soft and bright selected sources.

If completely identified flux limited samples are obtained using catalogue cross-correlation or work at the telescope, then the probability that X-ray emission from a given source originates from a particular class of emitters (star, AGN, etc.) may be eventually estimated in a quantitative manner. This allows the computation of a statistical identification using as input the restricted set of multi-wavelength parameters available for all sources.

RGPS sources identified in SIMBAD are far from making a complete sample. SIMBAD is roughly optical flux

limited, although at very different levels depending on the nature, stellar or extragalactic, of the object. As most of the recent additions are coming from the literature, the whole collection is highly heterogeneous. Clearly, the set of SIMBAD identifications cannot be used to provide real probabilities of identification. However, it may be used to construct selected samples of presumably enhanced probabilities.

A first analysis was made in 1991, using X-ray and optical characteristics of a limited number of stars, AGN, CVs and accreting binaries identified in preliminary and partial releases of the RASS. The selection criteria used to build the source samples studied in this paper are derived from this early analysis.

The recently published ROSAT all-sky survey bright source catalogue (BRASS) by Voges et al. (1996) constitutes a sample of larger size and of much better quality than the one originally used in 1991. Therefore, for the sole aim of illustrating in an extensive manner the X-ray selection criteria used in this work, we decided to cross-correlate BRASS with SIMBAD. We underline that the associations between bright RASS sources and SIMBAD entries used in this paper have not been human screened and cannot be considered individually as real identifications. Nevertheless their overall statistical properties may still be used for our purpose.

The BRASS covers the whole sky whereas the RGPS is by definition limited to the galactic plane area. However, selection rules arising from the BRASS catalogue can usefully be applied to the restricted RGPS area. The variability of parameters with galactic latitude or  $N_H$  can also be better studied using the whole sky catalogue.

The first step of the cross-correlation consisted in extracting from SIMBAD all objects located within  $3'$  from the ROSAT source, retrieving the optical position and associated error, the first identifier, possible ROSAT name, optical magnitudes, spectral types, full object type, number of references and Einstein measurements when available. In a second step, we retained from the SIMBAD cross correlation log entries having a non null intersection between the ROSAT 90% confidence circle and the SIMBAD error circle. As the error radius of Einstein sources is underestimated in SIMBAD, we updated it manually to  $50''$ . When several SIMBAD objects remained, we retained the one closest to the X-ray position. With a mean 90% error radius of  $27''$  for BRASS sources, and a total number of  $\sim 1.46 \cdot 10^6$  SIMBAD objects having in most cases small positional errors ( $\leq 1''$ ), we expect about 120 spurious matches between a SIMBAD and a ROSAT source. This estimate ignores effects resulting from inhomogeneities in the surface density of SIMBAD and BRASS entries. We list in Table 1 some statistics of the cross-correlation.

Clearly, the large majority of SIMBAD matches are real since only  $\sim 1.5\%$  of the sources with one or more SIMBAD entries are expected to be spurious. Considering the restrictive aim of this work, we did not investigate

**Table 1.** BRASS-SIMBAD correlation

Sample	Number	fraction of Total BRASS (%)
Unidentified	10705	56.9
1 SIMBAD match	6123	32.6
2 SIMBAD matches	1313	6.9
$\geq 3$ SIMBAD matches	670	3.6

in detail the reasons explaining the relatively large number of sources with multiple SIMBAD matches. Probably, the high surface density of SIMBAD entries in some specific small regions of the sky, multiple stellar systems and overall the fact that a number of astrophysical objects still appear as distinct SIMBAD objects could account for this effect.

Most of the proposed SIMBAD identifications of BRASS sources (61%) are with stars and only 20% with external galaxies and AGN. The high identified stellar fraction obviously reflects the emphasis put on stars in SIMBAD.

The quality of the cross-correlation may be judged from Fig. 1 which shows the relation between Einstein IPC and ROSAT PSPC count rates for the 1244 Einstein sources recovered in the BRASS. The ratio of the count rates of the two instruments strongly depends on source spectrum with an additional scatter due to variability. We show for comparison two lines (PSPC = 1  $\times$  IPC and PSPC = 6  $\times$  IPC corresponding to hard (power law photon index = 0) and soft (thermal spectra with  $\log T = 5.8$ ) sources respectively). As expected, most sources lie between these two extreme relations. The outstanding source at IPC = 0.02  $\text{cts s}^{-1}$  and PSPC = 20  $\text{cts s}^{-1}$  is the low-mass X-ray binary transient EXO 0748-676 which was detected by Einstein in the low state before its discovery by EXOSAT in outburst.

## 2.2. X-ray and optical properties of identified BRASS sources

For source classification purposes, the most interesting parameters are flux ratios in various energy bands, including the conventional X-ray hardness ratios, but also  $F_X/F_{\text{opt}}$  ratios as well as optical colours. Another important information for galactic studies is the line of sight absorption which can be estimated from HI and CO data.

Arguments involving the  $F_X/F_{\text{opt}}$  ratio have been used by many authors in the context of the Einstein Observatory surveys at high and low galactic latitudes (e.g., Maccauro et al., 1982; Hertz & Grindlay 1984). ROSAT offers a slightly improved spectral response compared to Einstein and allows PSPC hardness ratios to be used as additional information, at least for relatively bright sources.

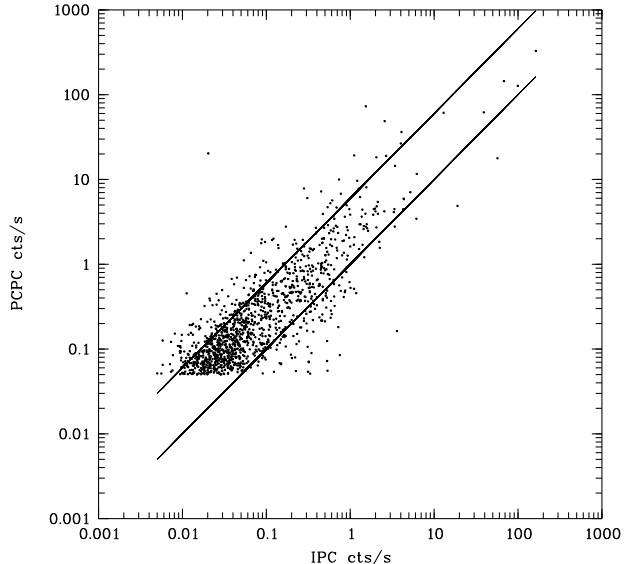


**Fig. 1.** The relation between Einstein IPC and PSPC count rates for 1244 Einstein sources identified with BRASS entries. The two lines represent the relation expected for soft and hard sources.

### 2.2.1. Hardness ratios

We plot in Fig. 2 the positions in the hardness ratio diagram of BRASS sources cross-identified in SIMBAD with different classes of objects.

The exact energy range used for the computation of hardness ratios changes with the version of the Scientific Analysis System Software (SASS; Voges et al., 1992). Whereas the 93 sources discussed in this paper were the output of SASS-I (see section 3.1), the BRASS catalogue (Voges et al. 1996) uses SASS-II processing in which the hardness ratios are defined as:

$$\text{HR1} = \frac{(0.5 - 2.0) - (0.1 - 0.4)}{(0.1 - 0.4) + (0.5 - 2.0)} \quad (\text{SASS - II})$$

$$\text{HR2} = \frac{(1.0 - 2.0) - (0.5 - 1.0)}{(1.0 - 2.0)} \quad (\text{SASS - II})$$

where (A-B) is the raw background corrected source count rate in the A–B energy range expressed in keV.

Active coronae populate the central part of the HR1/HR2 diagram with some tail extending towards hard spectra. Stellar coronae are known to exhibit a range of temperatures between  $3 \times 10^6$  K and  $10^7$  K, with the most active and luminous stars also exhibiting the highest kT and hardest spectra. In this diagram, isolated white dwarfs are all found at  $\text{HR1} \leq -0.9$ . At the BRASS flux level, the vast majority of active coronae are located within 100 pc from the Sun (e.g. Guillout et al. 1996b) and except for the early type stars and some of the most luminous late type binaries, the effects of interstellar absorption are negligible in both X-ray colours.

In general, the AGN found in SIMBAD do not exhibit HR2 smaller than  $\approx -0.2$  but have a large scatter in HR1 which is closely related to galactic foreground absorption (see below). However, ROSAT has discovered some AGN with very steep spectra which are so far barely represented in SIMBAD (e.g. Greiner et al. 1996).

The bulk of the cataclysmic variables populate the upper right quadrant, avoiding very hard HR2 values. Among outstanding sources we find at  $HR1 = 0.95 \pm 0.05$  and  $HR2 = -0.63 \pm 0.08$  the peculiar soft IP candidate RX J1914.4+2456 which exhibits strong interstellar absorption (Haberl & Motch, 1995; Motch et al. 1996). The supersoft X-ray emission from GQ Mus = Nova Muscae 1983 at  $HR1 = -0.05 \pm 0.27$  and  $HR2 = -0.87 \pm 0.47$  was discovered by Ögelman et al. (1993). Cataclysmic variables with  $HR1 \leq 0.1$  are all polar or soft intermediate polar systems.

Most X-ray binaries exhibit very hard X-ray hardness ratios resulting both from the usually high interstellar absorption towards these remote sources and from an intrinsically hard spectrum ( $kT \geq 2$  keV with sometimes local photoelectric absorption such as in Be/X-ray binaries for instance). The two objects at the lower left corner are supersoft sources in the Large Magellanic Cloud. The galactic supersoft source RX J0925.7-4758 ( $HR1 = 1.00 \pm 0.01$  and  $HR2 = -0.36 \pm 0.08$ ) exhibits an intrinsically soft spectrum affected by strong interstellar absorption. The source at  $HR1 = 0.64 \pm 0.02$  and  $HR2 = 0.09 \pm 0.02$  is the LMC transient 1A 0538-66 and that at  $HR1 = 0.20 \pm 0.03$  and  $HR2 = 0.31 \pm 0.04$  is the peculiar M giant binary HD 154791/A 1704+241.

### 2.2.2. Hardness ratios and $F_X/F_{opt}$

The most informative diagrams are without doubt those involving optical information, basically in the form of the  $F_X/F_{opt}$  ratio. The X-ray to optical flux ratio can be defined as  $\log(F_X/F_{opt}) = \log(\text{PSPC count rate}) + V/2.5 - 5.63$ , following the expression used by Maccacaro et al. (1982) for the Einstein medium sensitivity survey and assuming an average energy conversion factor of 1 PSPC cts  $s^{-1}$  for a  $10^{-11}$  erg  $cm^{-2}$   $s^{-1}$  flux in the range of 0.1 to 2.4 keV. We show in Fig. 3 the position of stars, AGN, X-ray binaries and cataclysmic variables in the X-ray colour versus  $F_X/F_{opt}$  ratio diagram.

Although stars and AGN have similar X-ray colours, their mean X-ray to optical ratios are obviously quite different and the two populations are well separated in the  $HR1/2$   $F_X/F_{opt}$  diagram. X-ray binaries are essentially recognizable from their hard X-ray spectra and usually large  $F_X/F_{opt}$ . The low  $F_X/F_{opt}$  X-ray binary tail consists of high mass X-ray binaries. Cataclysmic variables exhibit a large range of X-ray colours and  $F_X/F_{opt}$  ratios and can be somewhat confused with both the AGN and the most active part of the stellar population. However, the addition of a B-V or U-B optical index would allow

to distinguish further between these overlapping populations.

### 2.2.3. Interstellar absorption

An efficient way to discriminate between local and remote populations of X-ray sources is to use the anisotropy produced by the Galaxy, essentially in terms of scale height and interstellar absorption. This effect is illustrated in Figs. 4 and 5 which display the position of AGN, CVs and X-ray binaries in the integrated HI / hardness ratio diagram.

Most active stars detected in the RASS are little affected by interstellar absorption and their X-ray colours do not vary with galactic latitude (or integrated column density).

Apparently, the shape of the low energy spectrum of AGN is rather constant with the consequence that hardness ratio 1 is well correlated with the integrated HI column density as shown in Fig. 4. Actually, this relation is well defined and we used it for preselecting AGN candidates with a high rate of success. However, the HR2 distribution is relatively peaked around a value of 0.1 and does not vary with  $N_H$ . This is probably due to a selection effect against highly absorbed AGN which are likely to be missing in the mostly optically selected SIMBAD sample.

With X-ray luminosities up to  $10^{32-33}$  erg  $s^{-1}$ , cataclysmic binaries can be detected to distances as large as 1 kpc or more at the BRASS sensitivity. There is indeed a slight tendency that cataclysmic variables exhibiting the hardest HR1 are preferentially found at low galactic latitudes but the large variety of spectra emitted in this class (from very soft polars to intrinsically absorbed intermediate polars) somewhat blurs the picture.

In contrast, luminous X-ray binaries are seen by ROSAT at very large distances in deeply absorbed regions of the galactic plane and apart from a few cases (e.g. supersoft sources), their hardness ratio HR1 is close to +1, indicating that all X-ray photons below 0.4 keV are blocked by interstellar absorption. Effects of interstellar absorption are also seen on hardness ratio HR2 which involves higher energy bands. Not surprisingly, Fig. 5 shows that sources lying in the most absorbed direction of the Galaxy (and therefore lower galactic latitudes) are also the hardest in HR2.

## 3. Identification of sources from the ROSAT Galactic Plane Survey

### 3.1. The RGPS source list

The 93 sources discussed in this paper were extracted from the RGPS source list using selection criteria described in section 3.5 below. The RGPS source list results from the survey reduction performed by SASS-I in October 1991. This RASS reduction has well known documented flaws, namely a PSPC count rate overestimated by a factor of

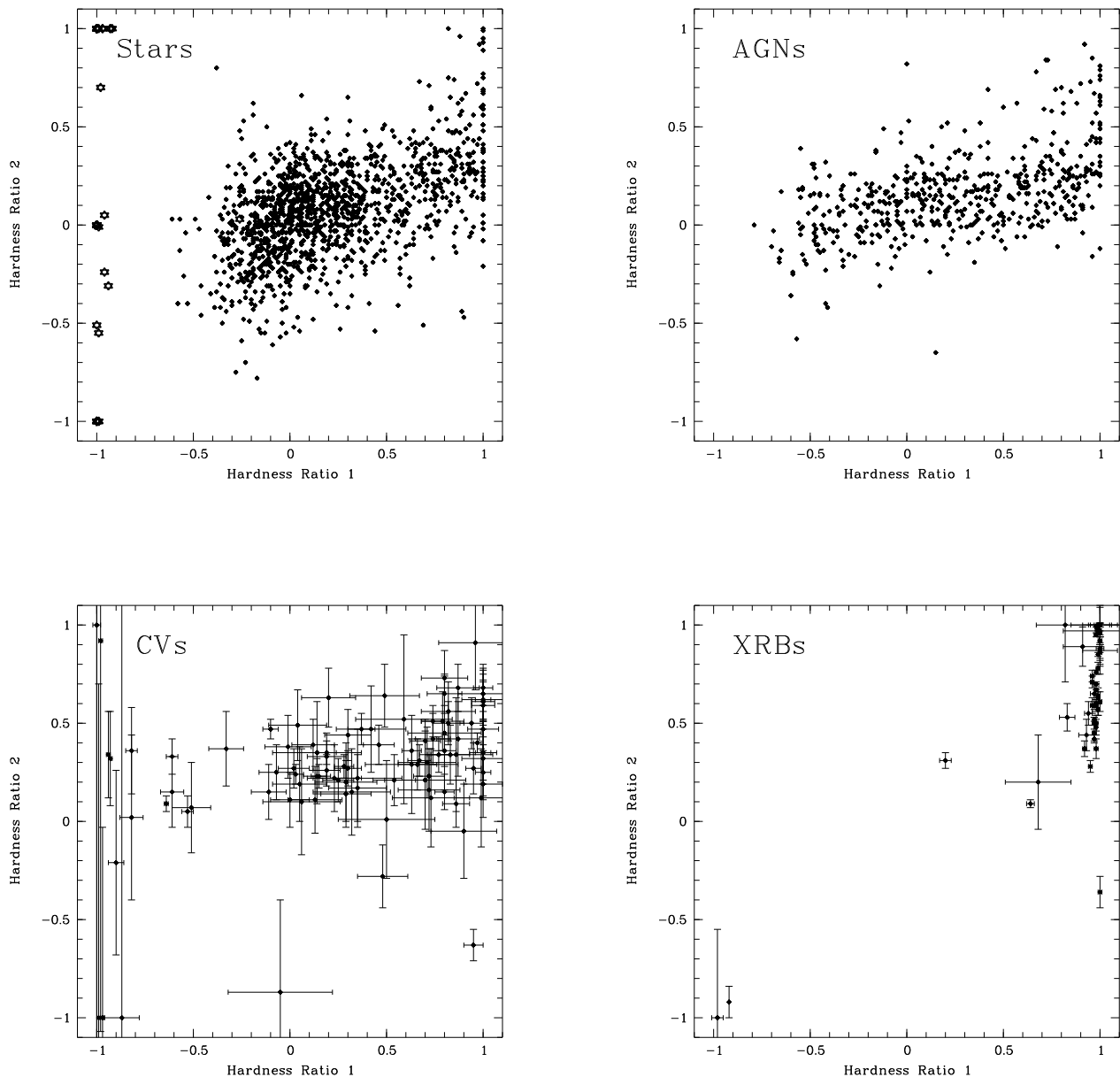


**Fig. 2.** Position of various classes of X-ray emitters in the HR1 HR2 diagram. Asterisks in the Stars diagram represent white dwarfs. The scatter in HR2 of white dwarfs is due to the large error on this ratio for such soft sources. For non-degenerate stars and AGN, we only show sources with errors less than 0.2 on both ratios.

$\approx 1.2$ , the appearance of some ghost sources caused by problems in the satellite attitude reconstruction in spinning mode and uneven sensitivity due to the strip accumulation.

Spacecraft problems prevented the detection of sources between ecliptic longitudes  $41^\circ$  and  $49^\circ$  and ecliptic longi-

tudes  $221^\circ$  and  $229^\circ$  leaving about 5% of the galactic sky without coverage.

The 1991 SASS-I version stacked photons in  $2^\circ$  wide strips along the great scan circles resulting in frequent multiple detections of the same source in adjacent strips. The lists of sources derived from each strip were merged into a single master list totaling about 15,000 sources at

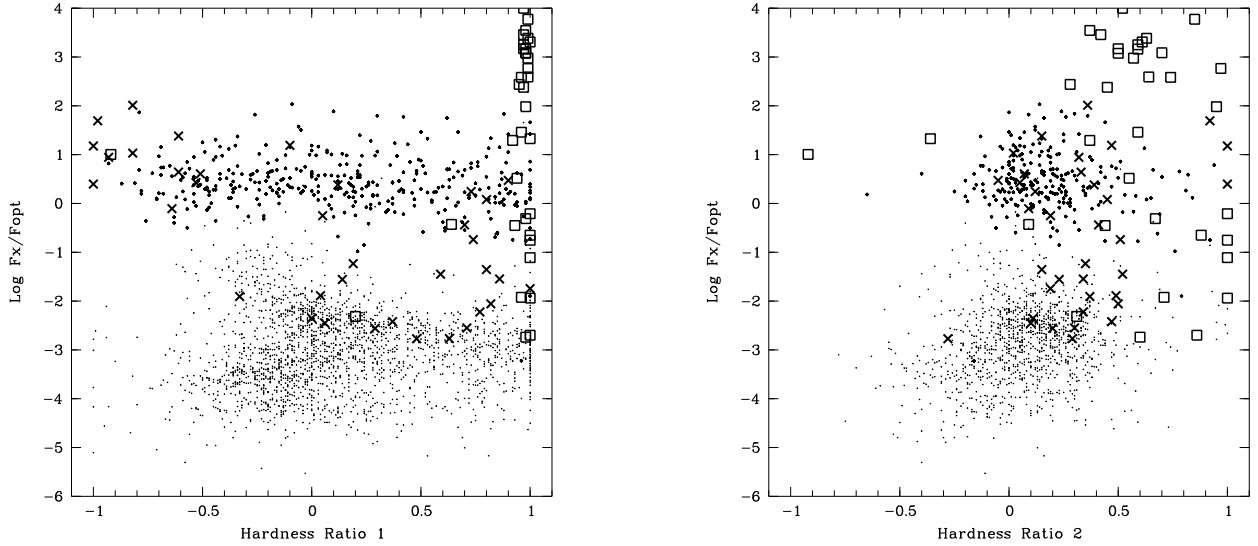


**Fig. 3.** The position of various classes of identified BRASS sources in the HR1 (left) or HR2 (right) /  $\text{Log}(F_X/F_{\text{opt}})$  diagram. Small dots represent stars, large dots AGN, squares are X-ray binaries and crosses are cataclysmic variables. For stars and AGN only sources having errors on HR1 smaller than 0.2 are plotted

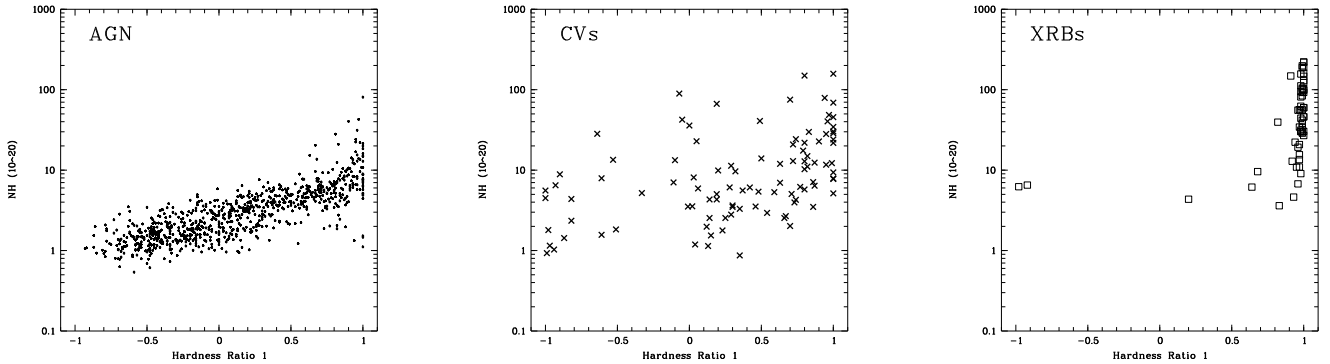


**Fig. 4.** Variation of HR1 with the integrated galactic HI column density for various classes of X-ray emitters. For stellar and AGN identifications, only sources with error on HR1 smaller than 0.2 are plotted

$|b| \leq 20^\circ$ . This list constitutes the database for the RGPS. Details on the merging procedure can be found in Motch et al. (1997b).

Errors on ROSAT X-ray positions are quadratic sums of the statistical uncertainty with which the centroid of the X-ray image is positioned on the pixel grid by the Maximum Likelihood source detection algorithm and of a systematic attitude error, estimated to be of the order of  $8''$  (Motch et al. 1997b).

Among the 93 sources, a total of 87 are bright enough to be also found in the RASS bright source catalogue (1 RXS, Voges et al. 1996) discussed in the previous section. The SASS process used for the production of the bright source list (SASS-II) detects sources on square sky areas, eliminating thus the uneven sensitivity resulting from the strip approach used in 1991. Updated attitude reconstruction removed ghost sources sometimes present in the 1991 version and human data screening ensured high quality. Most RGPS and BRASS positions are fully consistent

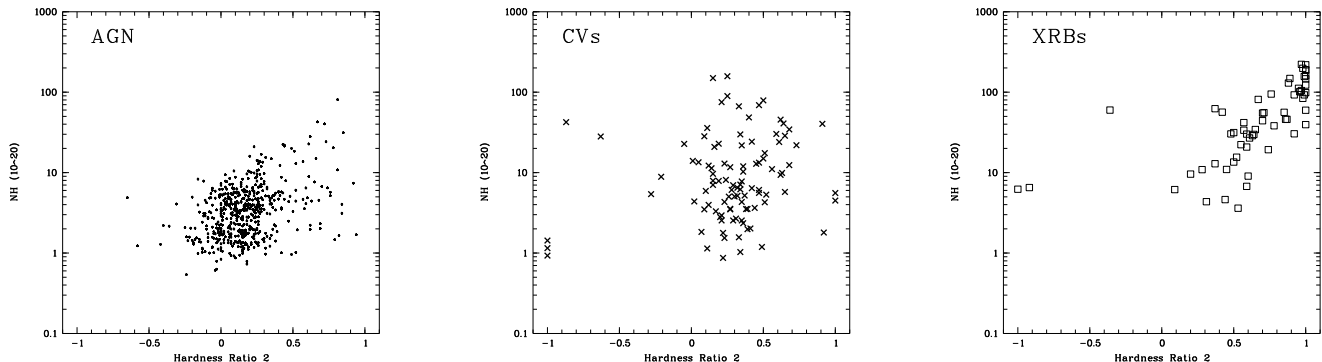


**Fig. 5.** Variation of HR2 with the integrated galactic HI column density for various classes of X-ray emitters. For stellar and AGN identifications, only sources with error on HR1 smaller than 0.2 are plotted

with a median difference in position of  $7.6''$ . The 90% confidence radii are similar. In a few cases mentioned below in the notes on individual objects, the offset between the RGPS and BRASS positions is significantly larger than  $r_{90}$  probably because of the use of an improved attitude solution in the SASS-II reduction. The 1991 SASS-I reduction also uses slightly different energy ranges than the SASS-II reduction for computing hardness ratios 1 and 2:

$$\text{HR1} = \frac{(0.40 - 2.40) - (0.07 - 0.40)}{(0.07 - 2.40)} \quad (\text{SASS - I})$$

$$\text{HR2} = \frac{(1.00 - 2.40) - (0.40 - 1.00)}{(0.40 - 2.40)} \quad (\text{SASS - I})$$

where (A-B) is the raw background corrected source count rate in the A–B energy range expressed in keV. There is no one to one relation between SASS-I and SASS-II hardness ratios as their values depend on the details of the observed count distribution in energy. However, a meaningful mean relation exists which can be used to propagate the ranges from one reduction to the other.

### 3.2. Optical observations

Optical material was collected at the Observatoire de Haute-Provence, CNRS, France for northern sources and at ESO, La Silla for the southern sky. The present observational material was acquired during several runs dedicated to the identification of ROSAT galactic plane survey sources in general which were carried out from 1991 till 1995 by various observers.

At OHP, multicolour CCD imagery was usually obtained with the 1.2m telescope few days before the spectroscopic run with the 1.9m. In most cases we used B and I band filters with additional U band exposures in a few instances. Pixel size was 0.85 or 0.77 arcsec on the sky

depending on the CCD chip used. At the 1.9m telescope, we operated the CARELEC spectrograph (Lemaitre et al. 1990). Most of the time we used two dispersions, a low resolution mode  $260 \text{ \AA/mm}$  ( $\lambda\lambda 3500 - 7500 \text{ \AA}$ ; FWHM resolution  $\approx 14 \text{ \AA}$ ) and a medium resolution mode in the blue  $33 \text{ \AA/mm}$  ( $\lambda\lambda 3800 - 4300 \text{ \AA}$ ; FWHM resolution  $\approx 1.8 \text{ \AA}$ ).

ESO data were acquired at the occasion of four runs in May 1991, April 1992, February 1994 and February 1997. In 1991, 1994 and 1997, we used the Boller & Chivens spectrograph at the ESO 1.5m telescope. Medium dispersion gratings were used in all cases yielding a FWHM resolution of  $4\text{-}5 \text{ \AA}$  and a wavelength range  $\lambda\lambda 3900 - 7200 \text{ \AA}$ . In 1992 we used EFOSC 2 at the ESO-MPI 2.2 m telescope with the same instrumental setting as described in Motch et al. (1994).

All spectral and photometric data reductions were performed using standard MIDAS procedures (Banse et al. 1983). Spectra were corrected for bias and flat-field and later calibrated in wavelength using arc lamps. In most cases we could acquire flux standard stars. However, uncertain weather conditions and the narrow slit entrance width sometimes used may introduce large errors in the derived flux.

### 3.3. Optical data analysis

For active coroneae, spectral classification was carried out as outlined in Motch et al. (1997a) using Turnsheck et al. (1985), Jacoby et al. (1984) and Jaschek & Jaschek (1987) stellar atlases.

Visual magnitudes were in most cases not derived from our CCD imagery as they usually lacked photometric calibration. Instead we used magnitudes extracted from the SIMBAD database, the Guide Star Catalogue (Lasker et al. 1990) or for the faintest counterparts, from the USNO-A1 catalogue (Monet 1997). The GSC magnitudes of stars

having a spectral type were corrected for colour effects according to relation (1) of Russell et al. (1990) assuming a main sequence unreddened object. After colour correction, the remaining  $1\sigma$  error on magnitudes is  $\approx 0.2$  mag.

The coordinates of the optical counterparts were in first priority extracted from the SIMBAD database which usually gives entries from astrometric catalogues (e.g. PPM). When no accurate SIMBAD positions were available we used the GSC coordinates and for the remaining identifications positions computed interactively using the Aladin sky atlas (Bonnarel et al. 1997) at the Centre de Données de Strasbourg (CDS).

The Aladin project aims to provide multi wavelength cross-identification. This tool is designed as an interactive X-window client accessing images from the CDS image server, Simbad database, CDS catalogue server and on-site catalogues. The Aladin collection contains a high resolution image archive of Schmidt plates digitized by the Paris MAMA facility and covering a significant portion of the sky, mainly in the Magellanic Clouds and southern Galactic Plane. The integration of the STScI Digital Sky Survey -1 in the system provides full-sky coverage albeit with a lower spatial resolution and astrometric accuracy than that of the MAMA archive. For the plates digitized by the MAMA, astrometric calibration is based on PPM standards and reaches an accuracy better than  $0.3''$  rms.

### 3.4. Optical identifications

The strategy used for optical identification of ROSAT sources in the galactic plane has been extensively discussed in Motch et al. (1997a). For stars, we used two criteria based on the Ca II H&K or H $\alpha$  flux to X-ray flux ratio and a priori probability of positional coincidence in the relatively small X-ray  $r_{90}$  of ( $\langle r_{90} \rangle = 25''$ ). The surface density of optically bright active galactic nuclei, cataclysmic variables, hot white dwarfs and Be stars is small enough that the discovery of one such object in the ROSAT error circle is highly significant.

When available, we show an optical spectrum of the identified counterpart, either low or medium resolution but in general, do not provide finding charts as the identifier and positions are in principle sufficient to localize the object. However in few cases where the counterpart does not appear in the USNO catalogue we show finding charts. We also show finding charts for all accreting sources.

For the 17 cases where we failed to find the counterpart we show on a finding chart the observed candidates in order to ease further follow-up studies but do not plot the spectra.

By default, the finding charts are extracted from the STScI DSS-1 and the RGPS/SASS-I 90% confidence error circle is shown. In some instances where the DSS-1 data are not able to show the candidates because of crowding or extreme colours, we use instead our CCD images.

Comments on individual sources, spectra and finding charts are given in section 5.

### 3.5. Source selection

The group of sources studied here was extracted from the entire RGPS source list using four different selection criteria, hard, soft, absorbed soft and bright candidates, all based on SASS-I hardness ratios and count rates. In this paper, we present the optical work done on a subset of sources in each of the selected groups. Some optical identifications which have been already published in dedicated papers are not repeated here whereas work at the telescope is pursued for a number of other sources. To this X-ray selected samples, we add a couple of AGN extracted from not yet fully published lists of identifications in sample areas (e.g., GPS1-4; Motch et al. (1991), Taurus region; Guillout et al., (1996a)). Three other sources are from a so far barely investigated region located at  $l \sim 130^\circ$ .

Hard sources were defined as having  $HR1 \geq 0.7$  and  $HR2 \geq -0.1$  ( $HR1_{BRASS} \geq 0.65$  and  $HR2_{BRASS} \geq -0.15$ ) with the additional condition applied in most cases that integrated galactic absorption was larger than  $4 \cdot 10^{21}$  H atom  $\text{cm}^{-2}$ . The requirement of large galactic absorption was aimed at screening the extragalactic component and searching preferentially for galactic accreting binaries. Most of the sources have count rates larger than  $0.1 \text{ cts s}^{-1}$ .

Soft sources were defined as having  $HR1 \leq -0.4$  ( $HR1_{BRASS} \leq -0.75$ ) with a maximal error of 0.5 and a PSPC count rate  $\geq 0.1 \text{ cts s}^{-1}$ . Such soft sources do not emit much at energies higher than 0.4 keV and HR2 is therefore essentially undefined. We expected to preferentially find white dwarfs and in general low luminosity soft sources in this sample.

Absorbed soft sources were defined as having  $HR1 \geq -0.4$  and  $HR2 \leq -0.4$  ( $HR1_{BRASS} \geq -0.6$  and  $HR2_{BRASS} \leq -0.2$ ). This sample was designed to discover intrinsically soft luminous sources undergoing relatively large interstellar absorption as a result of their remote location.

Bright sources do not fall in any of the other hardness ratio ranges and have PSPC count rates larger than  $0.25 \text{ cts s}^{-1}$ .

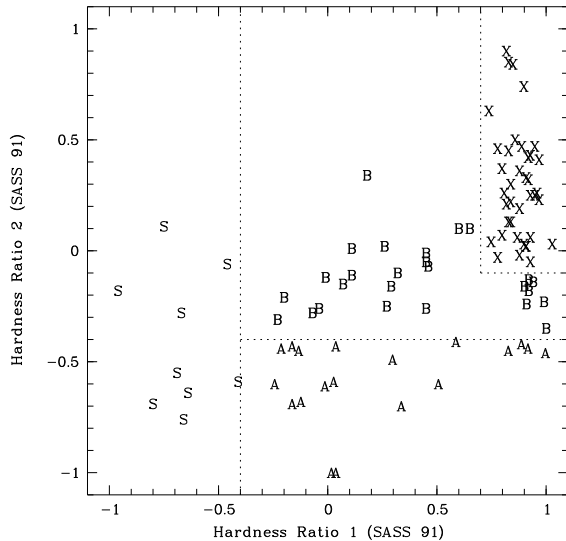
All samples were further cleaned by discarding those sources having an obvious identification in SIMBAD (catalogued X-ray source, bright active corona). However, in the course of this identification programme, some of these sources were recovered by other instrumentations (Sky Lab SLX, WFC RE, EUVE, etc.) or identified by other groups and now appear as such in SIMBAD.

We show in Fig. 6 the position of the various X-ray selected samples in the HR1/HR2 diagram and give number repartition by selection criteria in Table 2.

In Table 4 we list the RGPS source positions, count rates, hardness ratios and 1 RXS identification when avail-

**Table 2.** Repartition of the number of sources by selection criteria

Selection Criteria	Number of sources
Hard	39
Soft	9
Absorbed soft	19
Bright	17
Other	9

**Fig. 6.** Position of the various X-ray selected samples in the HR1/HR2 diagram. X = Hard X-ray binary like, A = Absorbed supersoft candidates, S = soft white dwarf candidates, B = remaining sources, mostly 'bright'

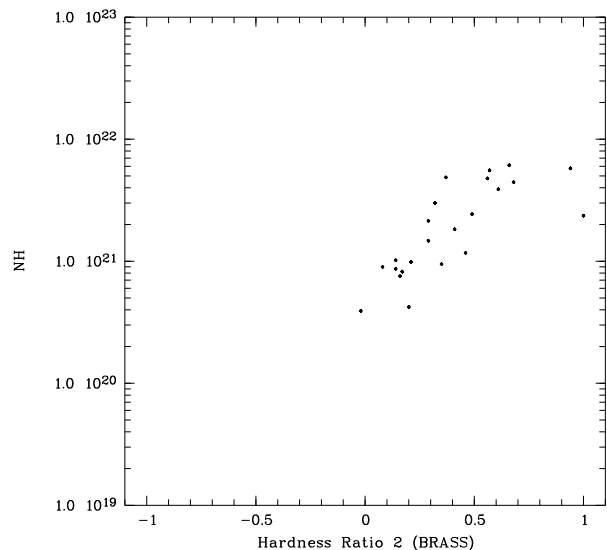
able. Table 5 gives optical identification, position, B and V when available. Spectra are shown in Fig. 8 and finding charts in Figs. 9 and 10.

### 3.5.1. Hard sources

Among the already published identifications of hard sources are the four CVs RX J0028.8+5917, RX J0744.9-5257, RX J1141.3-6410 and RX J2123.7+4217 (Motch et al. 1996). Some of the Be/X-ray candidates reported in Motch et al. (1997b) or the low-mass X-ray binary GS1826-24 identified in Barret et al. (1995) were also found in this sample. Here we report on the identification of RX J1739.5-2942 with a new Be/X-ray binary (see below). Our hard sample also contains the ultrasoft transient SLX 1746-331 (Skinner et al. 1990) which was apparently in outburst at the time of the ROSAT survey observation

in September 1990 and not detected in follow-up ROSAT HRI observations on 1994 October 2.

SIMBAD contains hardly any heavily absorbed AGN whereas all luminous galactic X-ray binaries, mostly discovered at higher energies are listed. This strong bias indicates that in hard X-ray selected samples, the number ratio of AGN to X-ray binaries or CVs should be much larger than suggested in Fig. 2, 4 and 5. A total of 13 AGN are indeed found in the hard sample, confirming that in the galactic plane, there is no easy way to disentangle absorbed AGN from genuine accreting binaries since both populations exhibit hard spectra and faint bluish counterparts. Not surprisingly, the new identified hard AGN are much more absorbed than the SIMBAD sample and their HR2 is correlated with NH (see Fig. 7). In 10 instances we identify the X-ray source with an optically bright active corona and in 13 cases, we fail to find a likely counterpart. Not unexpectedly, the vast majority of unidentified sources (13 among 17) are found in the hard sample and based on the properties of the identified population we can predict that most of these sources are likely to be absorbed extragalactic objects. In particular, from the lack of bright objects in I band images we can exclude relatively close Be/X-ray binaries as possible identification for these hard sources.

**Fig. 7.** Relation between hardness HR2 and galactic absorption for the newly identified AGN

### 3.5.2. Soft sources

The majority of the very soft sources discovered in the RASS turned out to be white dwarfs often also detected as bright UV sources in the Wide Field Camera Survey (Pounds et al. 1993) or by the Extreme Ultraviolet Explorer (Malina et al. 1994). Many of these bright sources were readily optically identified from their UV positions (Mason et al. 1995). Again, some active coronae emit low temperature X-ray spectra which are indistinguishable from white dwarf emission at the PSPC survey sensitivity.

Among the already published discoveries in this soft sample are the extremely hot PG 1159 star RX J2117.1+3412 (Motch et al. 1993) and the hot WD RX J2052.7+4639 (Motch et al. 1997a).

The other class appearing in this X-ray selected group is that of soft polars and intermediate polars in which the blackbody like X-ray emission from the polar cap dominates over the hard bremsstrahlung radiation from the shock in the accretion column (Beuermann & Schwöpe 1994, Haberl & Motch 1995). The polar RX J1802.1+1804 (Greiner et al. 1995) and RE 0751+14 (Mason et al. 1992, Motch & Haberl 1995) were also found in this sample. The exotic population of isolated neutron stars accreting from the interstellar medium should also show up as soft sources. In fact, two of the best candidates known so far were found in the soft sample (RXJ1856-37 Walter et al. 1996, RX J0720-3125 Haberl et al. 1997). RX J2102.0+3359 (see Tables 4 and 5) was also considered for some time as a good lone neutron star candidate. However, UB CCD imagery revealed the presence of a faint UV excess object ( $B=21.6$ ,  $U-B=-1.1$ ) close to the center of the error circle. This picture hints towards identification with an extreme  $F_X/F_{opt}$  ratio AM Her CV such as RXJ0453.4-4213 = RS Cae (Burwitz et al. 1996). However, its firm identification awaits optical spectroscopic confirmation.

In the soft sample presented here, we report the identification of a new DA white dwarf (RX J1936.3+2632 = 2EUVE J1936+26.5), 2 new polars (RX J0649.8-0737 and RX J0749.1-0549) of rather long orbital period and of a couple of active coronae.

### 3.5.3. Absorbed soft sources

Based on the obvious observation that no extremely X-ray bright soft source was found in the ROSAT survey nor in previous EUV surveys, we concluded that if a luminous supersoft source analogue to Cal 83 in the LMC were existing in the Galaxy, its observed X-ray spectrum would be dimmed and distorted by interstellar absorption. In order to delimit the range of hardness values to select, we simulated soft black body spectra affected by large interstellar absorption. With the ROSAT PSPC, large photoelectric absorption of a very soft source produces a very peaked

distribution centered at an energy which depends on the balance between  $kT$  and  $N_H$ .

Unfortunately, at the PSPC resolution, optically thin thermal spectra with many emission lines in the range of 0.3-0.5 keV can also produce peaked spectra, albeit with a much lower photoelectric absorption. Some active coronae may emit this kind of spectra in a narrow range of temperature and photoelectric absorption. Such spectra are also often seen in supernova remnants and in the hot diffuse galactic emission in general. Care was therefore taken to exclude extended X-ray sources by examining the survey images.

The first sample of absorbed soft sources in which we discovered the galactic supersoft binary RX J0925-4758 (Motch et al. 1994) and the peculiar intermediate polar candidate RX J1914.4+2456 (Motch et al. 1996) had more stringent constraints than set here ( $HR1_{SASS-I} \geq -0.4$  and  $HR2_{SASS-I} \geq -0.6$  with errors on HR1 and HR2 of less than 0.5 and 1.0 respectively and a count rate larger than  $0.1 \text{ cts s}^{-1}$ ). This restricted sample is now mostly identified and the remaining sources are associated with active stars.

Relaxing the constraints on HR2 increased the number of candidates but also the fraction of active coronae. Therefore, apart from one AGN (RX J1929.8+4622) and two CVs (RX J1951.7+3716 and RX J1946.2-0444), most sources are identified with stars. In three cases, however, we fail to identify the source. A fraction of these unidentified sources could be AGN with absorbed steep spectra.

### 3.5.4. Bright sources

A number of unidentified bright RGPS sources of high  $F_X/F_{opt}$  turned out to be previously unknown AGN or CVs. As shown in Fig. 3, selecting high  $F_X/F_{opt}$  sources at intermediate hardness ratios does improve the fraction of extragalactic and cataclysmic variable identifications. Some very active coronae with magnitudes below that of the limit of HD or SAO catalogues were also discovered.

## 4. Conclusions

The BRASS/SIMBAD cross-correlation and the set of optical identifications presented in this paper show that careful selection on multi-wavelength parameters can help to disentangle the various populations of X-ray sources accounting for the ROSAT survey.

In order to reach the state at which one can really compute probabilities of identification of any source with the main classes of X-ray emitters, large source samples have to be completely identified using catalogue data and proper multi-wavelength observations. In the galactic plane, the level of screening of the extragalactic population and in general galactic latitude are key parameters. Ideally, selected test samples should be accumulated at various latitudes in order to properly handle likelihoods

of identification such as for instance outlined in Sterzik et al. (1995).

Among the 93 selected sources, we find a likely counterpart to the X-ray source in 76 cases. With 39 identifications, active coronae again dominate source count. However, X-ray selection enhances the number of non-coronal identifications and we report on 25 new AGN, 6 new CVs, 2 new white dwarfs and a new Be/X-ray binary.

Our programme of optical identification of X-ray selected RGPS sources is going on and new identifications will be reported in a forthcoming paper. Statistics of identifications in the various selected samples will also be presented at this occasion.

## 5. Notes on individual objects

### 5.1. Stars

RX J0222.5+5033 = BD+49 646 : BD+49 646 was also detected by the ROSAT WFC (2RE J0222+503, Pye et al. 1995). The star GSC0330200570 located NE from BD+49 646 is a late A type star unrelated to the X-ray source.

RX J0621.2+4415 = G 101-35 : The BRASS error circle now encompasses the Me star. The star has high proper motion.

RX J0635.9+0755 = GSC0073302098 : The candidate star GSC0073302098 lacks the strong Ca II H&K emission which would be expected based on the PSPC count rate. However, the a priori probability of coincidence of the ROSAT source with the late G-K  $V \approx 10.7$  star is small enough so that the identification can be considered. The ROSAT source is identified with 2E 0633.2+075.

RX J0702.0+1257 = GSC0075701608 : Using EUVE data, Vennes et al. (1997) identify the source as a K0IV-V and a hot white dwarf in a wide binary. Part of the softness of the PSPC spectrum could be indeed explained by a contribution from the degenerate star. The XRT source is identical with EUVE J0702+129 and 2RE J0702+125 (Pye et al. 1995).

RX J0704.5-0612 = GSC0482603053 ?? : The brightest object in the RGPS error circle is GSC0482603053. A medium resolution spectrum of the star reveals Ca II H&K emission and some evidence for weak H $\alpha$  emission. Unfortunately, no absolute Ca II flux could be measured for this active corona, leaving some doubt on the compatibility of the chromospheric signature with the ROSAT X-ray flux. The second brightest object located SW from GSC0482603053 is a late type star without marked activity.

RX J0713.1-0511 = GSC0482302265 : The XRT source is identical to 2RE J0713-051.

RX J0721.3-5720 = GSC0855901016 + comp : The candidate M5eV star exhibits strong Balmer emission and is probably responsible for a large part of the X-ray emission. The close and comparatively bright star ( $V \approx 11$ )

GSC0855901016 is a main sequence K0 star. Unfortunately, we do not have Ca II H&K spectra which would have given indication on the level of stellar activity. The a priori coincidence of position between GSC0855901016 and a ROSAT survey source is small and could indicate that the bright star also contributes to the X-ray emission and constitutes a physical pair with the Me star.

RX J0811.1-5555 = GSC0857001980 : The absence of a spectrum covering the Ca II H&K region does not allow to firmly identify this source. However, in this case, the BRASS position which has a better accuracy than the RGPS determination, is centered on GSC0857001980 and excludes any other object than the  $V \approx 12$  late G star. This positional evidence and the soft X-ray hardness ratios suggest that GSC0857001980 is the counterpart of the ROSAT source.

RX J0828.5-5138 = GSC0816200330 : The BRASS position is now centered on the G star GSC0816200330. The low a priori probability of a random positional coincidence of the X-ray source with the relatively bright ( $V \approx 11$ ) star and the soft X-ray hardness ratio suggest a coronal identification.

RX J0845.7-3544 = GSC0714900583 : GSC0714900583 is a late G star, which considering the coincidence in position with the X-ray source and the soft X-ray spectrum is most probably the optical counterpart of the X-ray source.

RX J0856.4-2241 = GSC0658500334 : Weak Balmer emission may be present in the spectrum of GSC0658500334. The BRASS position is also centered on the early M star with a similar error radius. The soft X-ray spectrum is also consistent with a coronal identification.

RX J1704.3-4020 = HD 322763 : A follow-up HRI observation gives an improved position 17H04M17.68S -40D19M47.6S centered on the A star.

RX J2010.5+0632 = GSC0050701588 : The Me star is probably identified with the Parkes-MIT-NRAO survey source PMN J2010+0632 (Griffith et al. 1995). An X-ray flare was detected during the survey.

RX J2014.8+4501 = HD 192785 : The K0V star HD 192785 exhibits H $\alpha$  reemission (not shown) and was also detected in the Einstein Slew Survey (Schachter et al. 1996).

### 5.2. Active galactic nuclei

AGN identified in the low galactic latitude regions have all low redshift and the dominant population is Seyfert 1.

RX J0222.1+5221 = PMM1350-02324516 : This identification was already reported in Motch et al. (1991).

RX J0324.7+3410 = GSC0234901904 : This Seyfert 1 nucleus was independently discovered and identified with the HEAO-1 source H0321+340 by Remillard et al. (1993) and with the ROSAT source by Kock et al. (1996).

RX J0452.0+4932 = H0432052 : This object was already listed by Hauschildt (1987).

**Table 3.** Magnitude and redshift of newly identified AGN

Source Name	V/B	Type	$z$
RX J0222.1+5221	17.00	Sy 1	0.200
RX J0254.6+3931	16.10	BLRG	0.289
RX J0324.7+3410	15.10	Sy 1	0.063
RX J0325.2+4042	15.20	Sy 2:	0.048
RX J0337.0+4738	17.00	Sy 1	0.184
RX J0434.7+4014	15.20	Sy 1	0.021
RX J0452.0+4932	17.10	Sy 1	0.029
RX J0459.8+1808	19.50	Sy 1	0.157
RX J0508.3+1721	13.47	Sy 2:	0.017
RX J0508.9+2113	17.70	Sy 1	0.190
RX J0602.1+2828	15.00	Sy 1	0.033
RX J0608.0+3058	17.30	Sy 1	0.073
RX J0750.9+0320	15.20	Sy 1	0.099
RX J0755.7-0157	14.80	Sy 1	0.040
RX J0801.9-4946	11.07	Sy 1	0.040
RX J0816.4-1311	17.40	BL LAC	*
RX J0818.9-2252	15.50	Sy 1	0.035
RX J0913.0-2103	17.30	BL LAC	*
RX J1023.9-4336	17.50	BL LAC	*
RX J1741.4+0348	15.30	Sy 1	0.030
RX J1929.8+4622	17.00	Sy 1	0.127
RX J1931.1+0937	19.00	BL LAC	*
RX J2040.3+1059	16.10	Sy 1	0.085
RX J2043.9+5314	17.50	Sy 1	0.080
RX J2044.0+2833	14.70	Sy 1	0.050

RX J1931.1+0937 = A : Follow up ROSAT HRI observations revealed flare like activity by a factor of  $\approx 2$  on a time scale of one day. The best HRI position is 19H31M09.23S +09D37M18.96S with a conservative error radius of  $10''$ . The proposed optical counterpart displays a blue featureless continuum and is located within the  $1''$  radius error circle of the radio source NVSS J193109+093717. Based on these evidences we propose an identification with a BL Lac type of AGN.

RX J2040.3+1059 = PMM0975-19711620 : The AGN could be in an interacting system

### 5.3. Accreting sources

Detailed X-ray and, optical photometric and spectroscopic studies of the new CVs will be presented in future papers.

RX J0649.8-0737 = PMM0750-02887019 : This CV is a polar with a  $\approx 4.4$ h orbital period.

RX J0749.1-0549 = PMM0825-05603282 : This CV is a polar with a  $\approx 3.6$ h orbital period.

RX J1739.4-2942 = A : RX J1739.5-2942 is probably identical with GRS 1736-197 since the ROSAT position is located well within the  $90''$  radius of the 90% confidence circle of GRS 1736-197. The Be/X-ray nature of the source is consistent with the hard ART-P X-ray spectrum observed by GRANAT (Pavlinisky et al. 1994).

### 5.4. Miscellaneous and optically unidentified

RX J0035.8+5950 = ?? : None of the two GSC stars GSC0366601407 (A) and GSC0366600907 (B) lying at the edge of the ROSAT error circle exhibits detectable chromospheric activity.

RX J0529.0+0934 = ?? : Objects A and B display featureless continuum. B is bluer than A.

RX J0602.2+2837 = ?? : Object A has a featureless continuum. Object B could exhibit  $H\alpha$  emission.

RX J0620.6+2644 = ?? : The BRASS 90% confidence error area (small circle) does not overlap with the RGPS 90% error area. Because of the improved reduction process, the BRASS position should be considered as the best one. All objects A-E are late type stars without Balmer emission. A: late K, B: G-K, C: K, D: G-K and E: late G.

RX J0621.7+1747 = ?? : Object A is a late B type star, B a K type star and C a G-K type star.

RX J0648.7+1516 = ?? : The ROSAT source is identical to 1H 0646+152. A short exposure time spectrum of object A reveals a rather blue featureless continuum. B and C are probably late type stars.

RX J0717.4-1119 = ?? : The source was not recovered in a subsequent HRI pointing. Object A is a K type star and B has an A spectral type.

RX J0759.1+0748 = ?? : Bright X-ray source. Object A has an F-G spectral type and object B displays  $H\alpha$  and  $H\beta$  in absorption. Objects B and C have reddish featureless continua.

RX J0819.2-0756 = ?? : Objects A and B are F-G type stars. Object C is the only object visible inside the HRI position.

RX J1718.4-4029 = ?? : The image shown here is a 5 min I band CCD exposure obtained in April 1992 with EFOSC2 on ESO-MPI 2.2m. The HRI error circle (RA = 17H18M24.13S, -40D29M30.4S, 90% confidence radius =  $15.7''$ , 2000.0 eq) is plotted. Objects A,B and C display  $H\alpha$  and  $H\beta$  absorption lines.

RX J1740.7-2818 = ?? : The CCD image shown here is a 5 min I band exposure obtained with EFOSC2 and the MPI-ESO 2.2m telescope in April 1992. The field is heavily reddened. Objects A,B,C and D are late M stars without any noticeable Balmer emission.

RX J1742.3-2737 = ?? : The CCD image shown here is a 2 min I band exposure obtained with EFOSC2 and the MPI-ESO 2.2m telescope in April 1992. The field is heavily reddened. Object A is a reddened A-F type star and object B a reddened G-K star.

RX J1749.8-3312 = SLX 1746-331 : The CCD image shown here is a 5 min I band exposure obtained with EFOSC2 and the MPI-ESO 2.2m telescope in April 1992. The field is heavily reddened. Object A is a G-K type star.

RX J1749.8-3312 = 1RXS J174948.4-331215 is probably identified with the soft transient SLX 1746-331 (Skinner et al. 1990). The source was discovered by the Spacelab-2

coded-mask X-ray telescope in July-August 1985. Based on its ultrasoft spectrum and transient nature White & van Paradijs (1996) classify the source as a black hole transient. During the ROSAT survey observation (1990 Sep 08 23:15:57 to 1990 Sep 10 07:18:27) the source was caught in outburst and not detected during a subsequent ROSAT HRI follow-up observation (1994 Oct 2 from 05:58:58 to 06:30:40 UT). Considering the expected low mass of the companion star and high interstellar absorption on the line of sight, the optical identification is likely to be difficult outside X-ray outbursts.

RX J1804.1+0042 = PMM0900-11515260 : Follow-up ROSAT HRI observations show the source to be extended. Its mean position is 18H04M08.6S +00D42M26.3S, well centered on an extended optical object which could be an elliptical galaxy. A low S/N spectrum suggests a possible redshift of  $z = 0.07 \pm 0.02$ . The galaxy is probably identified with the Parkes-MIT-NRAO radio source PMN J1804+0042 (Brinkmann et al. 1997).

RX J1936.3+2632 = A : = 2EUVE J1936+26.5

RX J1943.9+2118 = ?? : We show a 10 min I band CCD exposure obtained in September 1995 with the 1.2 m telescope at OHP. The large error circle represents the RGPS localisation whereas the small one is derived from a follow-up ROSAT HRI observation. The HRI position is 19H43M56.16S +21D18M24.8S with a conservative error circle of  $10''$ . A is a reddened object without marked features apart from the Na I line and a possible Mg G band hollow. The position of A, 19H43M56.2S +21D18M20.4S is outside the error circle of the radio source NVSS J194356+211826 which is itself close to the center of the HRI error circle. The overall radio, optical and X-ray picture favors an heavily absorbed extragalactic identification.

RX J1950.0+3821 = ?? : Objects A, B, C and D are G type stars. The RGPS error circle contains a radio source NVSS J195004+382210 which is located  $\approx 8''$  north of A.

RX J2102.0+3359 = ?? UV excess object : We show here the BRASS position overlayed on a 10 min B filter CCD image obtained with the OHP 1.2 m telescope in September 1995. Object A is a late G early K star, B a G star. A low S/N spectrum reveals a featureless continuum for object C. Object X, located at 21H02M01.4S +33D59M29.6S exhibits a strong UV excess with  $B = 21.6$  and  $U-B = -1.1 \pm 0.3$ . The softness of the X-ray source and the presence of an UV excess object in the ROSAT error circle argue in favour of a AM Her system. Final identification should however await spectroscopic observations.

RX J2104.2+2118 = ?? : Objects A and B are late type stars. Object E displays a blue featureless continuum. The radio source NVSSJ210415+211805, is located in the RGPS and BRASS error circles,  $\approx 2''$  southern of object F.

RX J2156.3+3318 = PMM1200-18997159 : X-ray emission is slightly extended by 1 arcmin and centered on the presumably elliptical galaxy PMM1200-18997159 ( $z$

= 0.079, B=16.2, R=12.4). The fx/fopt ratio is compatible with normal emission from the galaxy without the need to add cluster contribution. The radio source NVSS J215623+331837 is coincident with the galaxy.

*Acknowledgements.* We thank the night assistants at Observatoire de Haute-Provence for carrying out some of the observations at the 1.2 m telescope. The ROSAT project is supported by the Bundesministerium für Bildung, Wissenschaft, Forschung und Technologie (BMBF/DLR) and the Max-Planck-Gesellschaft. C.M. acknowledges support from a CNRS-MPG cooperation contract and thanks Prof. J. Trümper and the ROSAT group for their hospitality and fruitful discussions. We are particularly grateful to the MPE team for providing early access to RASS data. This research has made use of the ALADIN sky atlas and of the SIMBAD database operated at CDS, Strasbourg, France. We thank F. Ochsenbein for providing easy access to the GSC and to the USNO-A1.0 catalogues. Finding charts were extracted from the *Digitized Sky Survey*, produced at the Space Telescope Science Institute (ST ScI) under U.S. Government grant NAG W-2166.

## References

- Banse, K., Crane, Ph., Ounnas, Ch., Ponz, D.: 1983, "MIDAS" in Proc. of DECUS, Zurich, p. 87
- Barret, D., Motch, C., Pietsch, W., Voges, W., 1995, A&A 296, 459
- Beuermann, K., Schwöpe, A.D., 1994, in: Interacting binary stars, ASP Conference Series Vol. 56, 119
- Beuermann, K., Reinsch, K., Barwig, H. et al., 1995, A&A 294, L1
- Bonnarel F., Ziaepour H, Bartlett J.G., Bienaymé O., Crézé M., Egret D., Florsch J., Genova F., Ochsenbein F., Raclot V., Louys M., Paillou P., 1997, IAU 179 Symposium proceedings, in press Eds Brain McLean.
- Brinkmann, W., Siebert, J., Feigelson, E.D., Kollgaard, R.I., Laurent-Mülsen, S.A., Reich, W., Fürst, E., Reich, P., Voges, W., Trümper, J., McMahon, R., 1997, A&A 323, 739
- Burwitz V., Reinsch K., Schwöpe A.D., et al., 1996, AA, 305, 507
- Greiner, J., Remillard, R., Motch, C., 1995, *IUA Circ* No. 6200
- Greiner, J., Danner, R., Bade, N., Richter, G. A., Kroll, P., Komossa, S., 1996, A&A 310, 384
- Griffith M.R., Wright A.E., Burke B.F., Ekers, R.D., 1995, ApJS 97, 347
- Guillout, P., Haywood, M., Motch, C., Robin, A.C., 1996a, MPE Report 263, 41
- Guillout, P., Haywood, M., Motch, C., Robin, A.C., 1996b, A&A 316, 89
- Haberl, F., Motch, C., 1995, A&A 297, L37
- Haberl, F., Motch, C., Buckley, D.A.H., Zickgraf, F.-J., Pietsch, W., 1997, A&A 326, 662
- Hauschildt, M., 1987, A&A 184, 43
- Hertz, P. Grindlay, J.E., 1984, ApJ 278, 137
- Jacoby, G.H., Hunter, D.A., Christian, C.A., 1984, ApJS 56, 257
- Jaschek, C., Jaschek, M., 1987, "The Classification of Stars", Press Syndicate of the University of Cambridge (USA)
- Kock, A., Meisenheimer, K., Brinkmann, W., Neumann, M., Siebert, J., 1996, A&A 307, 745

- Lasker, B.M., Sturch, C.R., McLean, B.J., Russel, J.L., Jenkner, H., Shara, M.M., 1990, *AJ* 99, 2019
- Lemaitre, G., Kohler, D., Lacroix, D., Meunier, J.P., Vin, A., 1990, *A&A* 228, 546
- Maccacaro, T., Feigelson, E.D., Fener, M., Giacconi, R., Gioia, I.M., Griffiths, R.E., Murray, S.S., Zamorani, G., 1982, *ApJ* 253, 504
- Malina, R.F., Marshall, H.L., Antia, B., et al., 1994, *AJ* 107, 751
- Mason, K.O., Watson, M.G., Ponman, T.J., Charles, P.Ap., Duck, S.R., Hassal, B.J.M., Howell, S.B., Ishida, M., Jones, D.H.P., Mittaz, J.P.D., 1992, *MNRAS* 258, 749
- Mason, K.O., Hassal, B.J.M., Bromage, G., et al., 1995, *MNRAS* 274, 1194
- Monet, D.G. et al., 1997, Publication of the US Naval Observatory Flagstaff Station
- Motch, C., Belloni, T., Buckley, D., Gottwald, M., Hasinger, G., Pakull, M.W., Pietsch, W., Reinsch, K., Remillard, R.A., Schmitt, J.H.M.M., Trümper, J., Zimmermann, H.-U., 1991, *A&A* 246, L24
- Motch, C., Werner, K., Pakull, M.W., 1993, *A&A* 268, 561
- Motch, C., Hasinger, G., Pietsch, W., 1994, *A&A* 284, 827
- Motch, C., Haberl, F., 1995, in proceedings of the Cape Workshop on Magnetic Cataclysmic Variables, ASP Conference Series, p109, Eds. D. A. H. Buckley and B. Warner
- Motch, C., Haberl, F., Guillout, P., Pakull, M., Reinsch, K., Krautter, J., 1996, *A&A* 307, 459
- Motch, C., Guillout, P., Haberl, F., Pakull, M.W., Pietsch, W., Reinsch, K., 1997a, *A&A* 318, 111
- Motch, C., Haberl, F., Dennerl, K., Pakull, M., Janot-Pacheco, E., 1997b, *A&A* 323, 853
- Ögelman, H., Orio, M., Krautter, J., Starfield, S., 1993, *Nat* 361, 331
- Pavlinisky, M.N., Grebenev, S.A., Sunyaev, R.A., 1994, *ApJ* 425, 110
- Pfeffermann, E., Briel, U.G., Hippmann, H., Kettenring, G., Metzner, G., Predehl, P., Reger, G. Stephan, K.H., Zombeck, M.V., Chappell, J., Murray, S.S., 1986, *SPIE* 733, 519
- Pounds, K.A., Allan, D.J., Barber, C., 1993, *MNRAS* 260, 77P
- Pye, J.P., Mc Gale, P.A., Allan, D.J., Barber, C.R., Bertram, D., Denby, M., Page, C.G., Ricketts, M.J., Stewart, B.C., West, R.G., 1995, *MNRAS* 274, 1165
- Remillard, R.A., Bradt, H.V.D., Brissenden, R.J.V., Buckley, D.A.H., Roberts, W., Schwartz, D.A., Stroozas, B.A., Tuohy, I.R., 1993, *AJ* 105, 2089
- Russel, J.L., Lasker, B.M., McLean, B.J., Sturch, C.R., Jenkner, H., 1990, *AJ* 99, 2059
- Schachter, J.F., Remillard, R., Saar, S., Favata, F., Sciortino, S., Barbera, M., 1996, *ApJ* 463, 747
- Skinner, G.K., Foster, A.J., Willmore, A.P., Eyles, C.J., 1990, *MNRAS* 243, 72
- Sterzik, M.F., Alcalá, J.M., Neuhäuser, R., Schmitt, J.H.M.M., 1995, *A&A* 297, 418
- Turnshek, D.E., Turnshek, D.A., Craine, E.R., Boeshaar, P.C., 1985, "An Atlas of Digital Spectra of Cool Stars", Western Research Company, Astronomy and Astrophysics Series, Volume 1
- Vennes, S., Christian, D.J., Mathioudakis, M., Doyle, J.G., 1997, *A&A* 318, L9
- Voges, W., 1992, in Proceedings of Satellite Symposium 3, 'International Space Year Conference', ESA ISY-3, 9
- Voges, W., Gruber, R., Paul, J., Bickert, K., Bohnet, A., Bursik, J., Dennerl, K., Englhauser, J., Hartner, G., Jennert, W., Köhler, H., Rosso, C., 1992, in Proceedings of Satellite Symposium 3, 'International Space Year Conference', ESA ISY-3, 1
- Voges, W., Aschenbach, B., Boller, T., Bräuninger, H., Briel, U., et al., 1996, *IUA Circ* No. 6420
- Walter, F.M., Wolk, S.J., Neuhäuser, R., 1996, *Nat* 379, 18
- White, N.E., van Paradijs, J., 1996, *ApJ* 473, L29
- Zickgraf, F.-J., Thiering, I., Krautter, J., Appenzeller, I., Kneer, R., Voges, W.H., Ziegler, B., Chavarria, C., Serrano, A., Mujica, R., Pakull, M., Heidt, J., 1997, *A&AS* 123, 103

**Table 4.** X-ray characteristics of ROSAT survey sources derived from the SASS as in October 1991. Coordinates are equinox 2000.0. The second column indicate the selection origin of the source as shown on Fig. 6, S, soft, A, absorbed soft, X, X-ray binary like, i.e. hard, B, remaining sources, mostly bright. Whenever the SASS-I RGPS source is bright enough to appear in the BRASS catalogue we give the 1RXS name

Source Name	Sel	Right Ascension	Declination	$r_{90}$ "	Cnt rate cts s <sup>-1</sup>	Error cts s <sup>-1</sup>	HR1	Error	HR2	Error	BRASS Name
RX J0035.8+5950	X	00H35M52.6S	59D50M08S	19.2	0.337	0.037	0.91	0.06	0.33	0.08	1RXS J003552.8+595006
RX J0119.0+7033	X	01H19M02.8S	70D33M09S	25.9	0.145	0.020	0.93	0.07	0.43	0.14	1RXS J011859.8+703336
RX J0143.7+6349	A	01H43M44.0S	63D49M30S	21.5	0.051	0.013	0.02	0.53	-1.00	9.99	1RXS J014343.7+634931
RX J0146.0+6348	A	01H46M05.8S	63D48M52S	21.5	0.054	0.017	0.04	0.71	-1.00	9.99	1RXS J014605.5+634853
RX J0202.2+6934	B	02H02M14.7S	69D34M23S	21.5	0.042	0.010	0.07	0.52	-0.15	0.52	
RX J0222.1+5221	X	02H22M06.9S	52D21M11S	25.9	0.174	0.028	0.86	0.13	0.50	0.15	1RXS J022206.0+522112
RX J0222.5+5033	B	02H22M35.0S	50D33M34S	18.4	0.422	0.034	-0.07	0.08	-0.28	0.11	1RXS J022234.1+503335
RX J0254.6+3931	B	02H54M41.8S	39D31M41S	20.3	0.121	0.020	1.00	9.99	-0.35	0.16	1RXS J025441.4+393143
RX J0256.3+6141	A	02H56M20.7S	61D41M24S	21.5	0.153	0.021	-0.01	0.14	-0.61	0.32	1RXS J025620.0+614129
RX J0324.7+3410	X	03H24M42.2S	34D10M51S	21.5	0.235	0.026	0.91	0.08	0.02	0.11	1RXS J032441.3+341056
RX J0325.2+4042	B	03H25M17.6S	40D42M00S	27.5	0.045	0.013	0.45	0.42	-0.01	0.53	
RX J0337.0+4738	X	03H37M04.0S	47D38M53S	21.5	0.134	0.021	0.83	0.16	0.13	0.17	1RXS J033703.9+473852
RX J0416.0+5237	A	04H16M03.0S	52D37M31S	22.9	0.102	0.025	-0.24	0.28	-0.60	0.45	1RXS J041602.7+523737
RX J0434.7+4014	X	04H34M42.2S	40D14M21S	19.2	0.197	0.024	0.84	0.15	0.22	0.13	1RXS J043442.1+401425
RX J0452.0+4932	X	04H52M05.0S	49D32M46S	17.7	0.595	0.048	0.92	0.07	0.42	0.06	1RXS J045205.0+493248
RX J0459.8+1808	B	04H59M51.2S	18D08M47S	38.5	0.061	0.014	0.60	0.33	0.10	0.26	
RX J0508.3+1721	X	05H08M20.6S	17D21M38S	22.9	0.064	0.018	0.89	0.10	0.47	0.40	1RXS J050820.9+172134
RX J0508.9+2113	X	05H08M55.7S	21D13M04S	31.0	0.058	0.018	0.88	0.12	-0.02	0.18	1RXS J050855.3+211304
RX J0529.0+0934	X	05H29M03.1S	09D34M38S	18.4	0.431	0.042	0.96	0.04	0.26	0.07	1RXS J052902.7+093439
RX J0535.0+6450	S	05H35M00.7S	64D50M47S	25.9	0.160	0.034	-0.75	0.22	0.11	0.70	1RXS J053501.1+645046
RX J0554.7+1055	A	05H54M45.8S	10D55M59S	21.5	0.193	0.033	-0.16	0.12	-0.69	0.27	1RXS J055446.0+105559
RX J0602.1+2828	X	06H02M10.6S	28D28M25S	18.4	0.708	0.057	0.97	0.03	0.23	0.06	1RXS J060210.7+282821
RX J0602.2+2837	X	06H02M17.5S	28D37M04S	25.9	0.149	0.031	0.93	0.06	-0.05	0.13	
RX J0608.0+3058	X	06H08M01.7S	30D58M53S	22.9	0.112	0.025	0.78	0.19	0.46	0.40	1RXS J060801.7+305847
RX J0620.6+2644	X	06H20M40.3S	26D44M28S	25.9	0.338	0.038	0.93	0.07	0.06	0.13	1RXS J062040.0+264339
RX J0621.2+4415	A	06H21M13.8S	44D15M47S	21.5	0.510	0.074	0.04	0.14	-0.43	0.19	1RXS J062113.1+441430
RX J0621.7+1747	X	06H21M47.8S	17D47M30S	19.2	0.113	0.021	0.84	0.15	0.30	0.46	1RXS J062148.1+174736
RX J0625.8-0101	S	06H25M49.8S	-01D01M40S	21.5	0.143	0.022	-0.46	0.16	-0.06	0.53	1RXS J062549.8-010138
RX J0635.9+0755	X	06H35M58.2S	07D55M28S	20.3	0.247	0.029	0.81	0.17	0.26	0.11	1RXS J063558.5+075527
RX J0648.7+1516	X	06H48M47.4S	15D16M26S	*	0.679	0.679	1.03	0.06	0.03	0.06	1RXS J064847.8+151626
RX J0649.8-0737	S	06H49M50.2S	-07D37M41S	21.5	0.557	0.055	-0.69	0.08	-0.55	0.36	1RXS J064949.8-073734
RX J0656.8-1424	X	06H56M53.6S	-14D24M56S	17.7	0.788	0.048	0.80	0.05	0.07	0.06	1RXS J065653.2-142455
RX J0702.0+1257	S	07H02M04.1S	12D57M50S	18.4	1.180	0.067	-0.67	0.04	-0.28	0.15	1RXS J070204.3+125758
RX J0704.5-0612	X	07H04M31.3S	-06D12M35S	24.3	0.113	0.021	0.78	0.20	-0.03	0.18	1RXS J070431.1-061224
RX J0713.1-0511	B	07H13M11.1S	-05D11M52S	17.7	1.470	0.069	-0.23	0.05	-0.31	0.07	1RXS J071311.0-051142
RX J0717.4-1119	X	07H17M25.1S	-11D19M43S	27.5	0.145	0.026	0.83	0.16	0.45	0.13	1RXS J071722.6-111954
RX J0721.3-5720	B	07H21M22.8S	-57D20M49S	32.8	0.199	0.020	-0.01	0.10	-0.12	0.13	1RXS J072123.9-572034
RX J0749.1-0549	S	07H49M09.7S	-05D49M31S	27.5	0.615	0.082	-0.80	0.18	-0.69	0.37	1RXS J074909.8-054933
RX J0750.9+0320	B	07H50M59.8S	03D20M18S	18.4	0.808	0.057	0.32	0.07	-0.10	0.09	1RXS J075100.0+032017
RX J0755.7-0157	B	07H55M47.3S	-01D57M48S	17.7	0.882	0.058	0.29	0.07	-0.16	0.09	1RXS J075547.4-015742
RX J0759.1+0748	A	07H59M09.0S	07D48M26S	21.5	3.360	0.200	-0.16	0.06	-0.43	0.09	1RXS J075908.8+074835
RX J0801.9-4946	X	08H01M57.8S	-49D46M42S	20.3	0.173	0.018	0.92	0.07	0.32	0.10	1RXS J080157.7-494639
RX J0811.1-5555	B	08H11M09.8S	-55D55M26S	36.5	0.125	0.014	0.18	0.11	0.34	0.16	1RXS J081108.7-555553
RX J0816.4-1311	B	08H16M26.7S	-13D11M46S	19.2	0.861	0.058	0.92	0.03	-0.13	0.08	1RXS J081626.9-131149
RX J0818.9-2252	X	08H18M57.3S	-22D52M32S	24.3	0.566	0.047	0.90	0.07	0.03	0.08	1RXS J081858.0-225229
RX J0819.2-0756	A	08H19M17.7S	-07D56M20S	20.3	0.158	0.029	0.83	0.16	-0.45	0.18	1RXS J081917.6-075620
RX J0828.5-5138	B	08H28M33.2S	-51D38M19S	25.9	0.236	0.021	0.11	0.10	-0.11	0.11	1RXS J082832.2-513828
RX J0845.7-3544	A	08H45M43.0S	-35D44M27S	22.9	0.077	0.016	0.34	0.46	-0.70	0.26	
RX J0856.4-2241	A	08H56M26.4S	-22D41M42S	25.9	0.102	0.025	0.30	0.48	-0.49	0.40	1RXS J085626.3-224141
RX J0913.0-2103	B	09H13M00.8S	-21D03M23S	17.7	0.924	0.052	0.94	0.02	-0.14	0.07	1RXS J091300.4-210315
RX J0935.5-2802	B	09H35M31.5S	-28D02M50S	21.5	0.267	0.031	-0.04	0.11	-0.26	0.17	1RXS J093530.9-280255
RX J1023.9-4336	B	10H23M55.5S	-43D36M03S	19.2	1.280	0.062	0.92	0.03	-0.18	0.05	1RXS J102356.4-433602
RX J1155.4-5641	B	11H55M27.7S	-56D41M59S	31.0	0.819	0.067	0.65	0.05	0.10	0.06	1RXS J115527.6-564149
RX J1606.6-4618	X	16H06M37.1S	-46D18M30S	31.0	0.139	0.025	0.84	0.15	0.13	0.17	1RXS J160637.1-461835
RX J1639.7-3920	X	16H39M47.8S	-39D20M15S	31.0	0.254	0.033	0.80	0.18	0.37	0.13	1RXS J163947.8-392023
RX J1704.3-4020	X	17H04M19.4S	-40D20M13S	21.5	0.214	0.039	0.88	0.12	0.36	0.13	1RXS J170419.7-402012
RX J1718.4-4029	X	17H18M24.2S	-40D29M34S	31.0	0.167	0.039	0.74	0.23	0.63	0.31	1RXS J171824.2-402934
RX J1739.4-2942	X	17H39M30.1S	-29D42M07S	19.2	0.154	0.030	0.85	0.14	0.84	0.15	1RXS J173930.3-294211
RX J1740.7-2818	X	17H40M42.8S	-28D18M03S	20.3	0.336	0.041	0.83	0.15	0.85	0.14	1RXS J174043.1-281806
RX J1741.4+0348	X	17H41M27.5S	03D48M48S	18.4	1.180	0.063	0.91	0.09	0.02	0.05	1RXS J174128.1+034848
RX J1742.3-2737	X	17H42M20.2S	-27D37M36S	24.3	0.166	0.033	0.90	0.10	0.74	0.22	1RXS J174220.8-273736
RX J1749.8-3312	X	17H49M48.3S	-33D12M26S	18.4	0.543	0.062	0.97	0.03	0.41	0.07	1RXS J174948.4-331215

*Continued on next page*

Source Name	Sel	Right Ascension	Declination	$r_{90}$ "	Cnt rate cts s <sup>-1</sup>	Error cts s <sup>-1</sup>	HR1	Error	HR2	Error	BRASS Name
RX J1804.1+0042	X	18H04M08.3S	00D42M29S	22.9	0.354	0.042	0.95	0.05	0.25	0.09	1RXS J180408.7+004229
RX J1925.0+4429	A	19H25M01.8S	44D29M43S	21.5	0.317	0.030	0.51	0.08	-0.60	0.08	1RXS J192502.2+442948
RX J1929.8+4622	A	19H29M50.1S	46D22M16S	21.5	0.392	0.030	0.59	0.09	-0.41	0.07	1RXS J192949.7+462231
RX J1931.1+0937	X	19H31M09.0S	09D37M22S	17.7	0.625	0.047	0.93	0.07	0.25	0.08	1RXS J193109.5+093714
RX J1935.4+3746	A	19H35M29.4S	37D46M09S	25.9	0.528	0.042	-0.13	0.08	-0.45	0.12	1RXS J193528.9+374605
RX J1936.3+2632	S	19H36M18.1S	26D32M42S	31.0	0.100	0.022	-0.64	0.30	-0.64	0.42	
RX J1943.9+2118	X	19H43M55.4S	21D18M15S	32.8	0.103	0.023	0.82	0.17	0.90	0.09	1RXS J194356.1+211731
RX J1946.2-0444	A	19H46M16.5S	-04D44M47S	21.5	0.114	0.026	1.00	9.99	-0.46	0.18	1RXS J194616.9-044456
RX J1947.3+3045	S	19H47M23.4S	30D45M55S	19.2	1.170	0.064	-0.96	0.03	-0.18	0.68	1RXS J194723.8+304558
RX J1950.0+3821	A	19H50M04.7S	38D21M52S	20.3	0.117	0.023	0.92	0.08	-0.44	0.16	1RXS J195005.2+382155
RX J1951.7+3716	A	19H51M46.2S	37D16M56S	27.5	0.102	0.023	0.89	0.11	-0.42	0.19	1RXS J195148.7+371712
RX J1953.6+5025	B	19H53M41.0S	50D25M03S	22.9	0.203	0.018	0.11	0.09	0.01	0.13	1RXS J195340.6+502456
RX J1956.7+5304	B	19H56M46.7S	53D04M31S	31.0	0.170	0.014	0.45	0.08	-0.26	0.10	1RXS J195646.5+530424
RX J2002.1+5438	B	20H02M07.9S	54D38M05S	31.0	0.435	0.023	0.27	0.05	-0.25	0.06	1RXS J200208.2+543827
RX J2010.5+0632	B	20H10M34.3S	06D32M06S	21.5	0.881	0.070	-0.20	0.08	-0.21	0.11	1RXS J201034.8+063208
RX J2014.8+4501	B	20H14M49.8S	45D01M32S	22.9	0.610	0.030	0.46	0.05	-0.07	0.06	1RXS J201449.4+450143
RX J2019.8+2256	A	20H19M48.9S	22D56M21S	18.4	0.523	0.037	-0.21	0.08	-0.44	0.11	1RXS J201949.3+225628
RX J2021.7+5213	A	20H21M44.2S	52D13M54S	25.9	0.071	0.011	0.03	0.37	-0.59	0.27	1RXS J202144.2+521348
RX J2033.4+3128	B	20H33M25.3S	31D28M03S	20.3	0.273	0.026	0.26	0.10	0.02	0.13	1RXS J203324.9+312816
RX J2040.3+1059	B	20H40M18.5S	10D59M40S	19.2	0.532	0.052	0.45	0.09	-0.05	0.11	1RXS J204019.1+105941
RX J2043.9+5314	X	20H43M59.4S	53D14M29S	21.5	0.229	0.018	0.95	0.04	0.47	0.07	1RXS J204400.1+531434
RX J2044.0+2833	B	20H44M03.9S	28D33M05S	19.2	0.303	0.030	0.91	0.06	-0.24	0.09	1RXS J204404.0+283303
RX J2102.0+3359	S	21H02M02.9S	33D59M22S	24.3	0.160	0.019	-0.66	0.12	-0.76	0.18	1RXS J210201.7+335932
RX J2102.6+4553	A	21H02M40.5S	45D53M05S	24.3	0.216	0.022	-0.12	0.10	-0.68	0.19	1RXS J210241.4+455305
RX J2104.2+2118	X	21H04M16.2S	21D18M20S	20.3	0.145	0.019	0.88	0.11	0.19	0.15	1RXS J210416.4+211816
RX J2109.7+4029	X	21H09M47.3S	40D29M47S	31.0	0.121	0.018	0.82	0.17	0.21	0.14	1RXS J210948.0+402944
RX J2133.7+5107	B	21H33M43.5S	51D07M20S	19.2	0.513	0.031	0.90	0.06	-0.16	0.06	1RXS J213344.1+510725
RX J2155.3+5938	S	21H55M21.0S	59D38M49S	34.7	0.112	0.024	-0.41	0.18	-0.59	0.32	1RXS J215522.8+593843
RX J2156.3+3318	B	21H56M23.3S	33D18M40S	22.9	0.516	0.042	0.99	0.01	-0.23	0.09	1RXS J215623.8+331829
RX J2255.0+5540	X	22H55M03.3S	55D40M53S	24.3	0.103	0.026	0.75	0.22	0.04	0.17	1RXS J225504.1+554052
RX J2322.6+6113	X	23H22M38.3S	61D13M29S	34.7	0.118	0.023	0.87	0.10	0.06	0.20	1RXS J232241.3+611335

**Table 5.** Optical identifications of ROSAT survey sources. The second column indicates the selection origin of the source as shown on Fig. 6, and given in Table 4. The last column indicates whether a finding chart is provided.

Source Name	Sel	d(x-o) (r <sub>90</sub> )	Right Asce.			Dec			Optical Identification	V	B	Class	Type	Finding Chart
			h	m	s	d	'	''						
RX J0035.8+5950	X	*	*	*	*	*	*	*	??	*	*	UNID		Y
RX J0119.0+7033	X	0.64	1	19	3.32	70	33	25.7	GSC0430101235	9.89	*	AC	K1V	
RX J0143.7+6349	A	1.09	1	43	43.57	63	49	54.0	HD 10436	8.41	*	AC	K5V	
RX J0146.0+6348	A	0.31	1	46	4.96	63	48	56.4	HD 10663	8.69	*	AC	G2V	
RX J0202.2+6934	B	0.09	2	2	14.60	69	34	21.1	GSC0431501020	11.72	*	AC	G2V	
RX J0222.1+5221	X	0.28	2	22	6.19	52	21	8.4	PMM1350-02324516	*	17.00	AGN	Sy 1	
RX J0222.5+5033	B	0.91	2	22	33.42	50	33	41.9	BD+49 646	10.10	*	AC	G2V	
RX J0254.6+3931	B	0.59	2	54	42.63	39	31	34.7	CJ2 0251+393	16.10	*	AGN	BLRG	
RX J0256.3+6141	A	0.21	2	56	20.11	61	41	22.6	GSC0404800621	13.08	*	AC	M2Ve	
RX J0324.7+3410	X	0.66	3	24	41.16	34	10	45.9	GSC0234901904	15.10	*	AGN	Sy 1	
RX J0325.2+4042	B	1.82	3	25	13.22	40	41	54.6	PMM1275-02314407	15.20	*	AGN	Sy 2:	
RX J0337.0+4738	X	0.42	3	37	3.14	47	38	51.5	PMM1350-03755404	*	17.00	AGN	Sy 1	
RX J0416.0+5237	A	0.35	4	16	3.54	52	37	37.8	GSC0371900494	11.70	*	AC	K7V	
RX J0434.7+4014	X	0.42	4	34	41.54	40	14	19.3	PMM1275-03482924	*	15.20	AGN	Sy 1	
RX J0452.0+4932	X	0.09	4	52	5.00	49	32	45.2	H0432052	17.10	*	AGN	Sy 1	
RX J0459.8+1808	B	0.34	4	59	51.90	18	8	38.9	PMM1050-01591537	*	19.50	AGN	Sy 1	
RX J0508.3+1721	X	0.71	5	8	19.72	17	21	48.1	GSC0128601162	13.47	*	AGN	Sy 2:	
RX J0508.9+2113	X	0.25	5	8	55.15	21	13	2.4	PMM1050-01718259	*	17.70	AGN	Sy 1	
RX J0529.0+0934	X	*	*	*	*	*	*	*	??	*	*	UNID		Y
RX J0535.0+6450	S	0.32	5	35	0.62	64	50	39.1	GSC0408900790	12.37	*	AC	K	
RX J0554.7+1055	A	0.09	5	54	45.87	10	55	57.9	GSC0072000052	11.93	*	AC	G0V	
RX J0602.1+2828	X	0.20	6	2	10.70	28	28	22.1	PMM1125-03274684	*	15.00	AGN	Sy 1	
RX J0602.2+2837	X	*	*	*	*	*	*	*	??	*	*	UNID		Y
RX J0608.0+3058	X	0.64	6	8	0.95	30	58	42.0	PMM1200-04416825	*	17.30	AGN	Sy 1	
RX J0620.6+2644	X	*	*	*	*	*	*	*	??	*	*	UNID		Y
RX J0621.2+4415	A	3.05	6	21	12.50	44	14	43.4	G 101-35	11.93	*	AC	M2Ve	
RX J0621.7+1747	X	*	*	*	*	*	*	*	??	*	*	UNID		Y
RX J0625.8-0101	S	0.34	6	25	49.51	-1	1	46.3	GSC0478501175	12.69	*	AC	M1Ve	
RX J0635.9+0755	X	0.35	6	35	58.28	7	55	21.0	GSC0073302098	10.69	*	AC	G-K	
RX J0648.7+1516	X	*	*	*	*	*	*	*	??	*	*	UNID		Y
RX J0649.8-0737	S	0.49	6	49	50.90	-7	37	40.2	PMM0750-02887019	*	18.00	CV		Y
RX J0656.8-1424	X	0.61	6	56	54.33	-14	24	59.0	GSC0539202173	9.77	*	AC	K0V	
RX J0702.0+1257	S	0.29	7	2	3.99	12	57	55.4	GSC0075701608	9.89	*	AC	Ke	
RX J0704.5-0612	X	0.75	7	4	31.46	-6	12	17.2	GSC0482603053 ??	13.00	*	AC??	G-K	
RX J0713.1-0511	B	0.53	7	13	11.22	-5	11	43.4	GSC0482302265	12.14	*	AC	M3Ve	
RX J0717.4-1119	X	*	*	*	*	*	*	*	??	*	*	UNID		Y
RX J0721.3-5720	B	0.42	7	21	23.76	-57	20	37.8	GSC0855901016 comp	11.23	*	AC	K0V+M5eV	
RX J0749.1-0549	S	0.47	7	49	10.45	-5	49	24.9	PMM0825-05603282	*	19.00	CV		Y
RX J0750.9+0320	B	1.46	7	51	0.73	3	20	40.9	PMM0900-05507668	*	15.20	AGN	Sy 1	
RX J0755.7-0157	B	0.36	7	55	47.32	-1	57	41.7	PMM0825-05763804	*	14.80	AGN	Sy 1	
RX J0759.1+0748	A	*	*	*	*	*	*	*	??	*	*	UNID		Y
RX J0801.9-4946	X	0.33	8	1	58.00	-49	46	36.0	ESO 209- 12	11.07	*	AGN	Sa Sy 1	
RX J0811.1-5555	B	0.82	8	11	9.37	-55	55	56.5	GSC0857001980	11.97	*	AC	G-K0	
RX J0816.4-1311	B	0.51	8	16	27.19	-13	11	52.6	PMM0750-06007988	*	17.40	AGN	BL LAC	
RX J0818.9-2252	X	0.28	8	18	57.70	-22	52	35.9	PMM0600-05866078	*	15.50	AGN	Sy 1	
RX J0819.2-0756	A	*	*	*	*	*	*	*	??	*	*	UNID		Y
RX J0828.5-5138	B	0.58	8	28	32.34	-51	38	32.6	GSC0816200330	10.87	*	AC	G	
RX J0845.7-3544	A	0.48	8	45	42.51	-35	44	36.6	GSC0714900583	12.09	*	AC	G-K	
RX J0856.4-2241	A	0.10	8	56	26.41	-22	41	39.8	GSC0658500334	12.41	*	AC	M0-1V(e)	
RX J0913.0-2103	B	0.51	9	13	0.17	-21	3	20.9	PMM0675-07248276	*	17.30	AGN	BL LAC	
RX J0935.5-2802	B	0.23	9	35	31.28	-28	2	54.0	GSC0660900298	12.08	*	AC	M0Ve	
RX J1023.9-4336	B	0.35	10	23	56.11	-43	36	2.5	PMM0450-11341838	*	17.50	AGN	BL LAC	
RX J1155.4-5641	B	0.27	11	55	27.03	-56	41	53.3	PMM0300-14373754	*	13.60	CV		Y
RX J1606.6-4618	X	0.18	16	6	36.75	-46	18	26.6	GSC0831000256	12.03	*	AC	G-K	
RX J1639.7-3920	X	0.83	16	39	47.29	-39	20	40.3	GSC0785402093	13.29	*	AC	M0Ve	
RX J1704.3-4020	X	1.32	17	4	17.93	-40	19	50.2	HD 322763	10.60	*	AC	A3	
RX J1718.4-4029	X	*	*	*	*	*	*	*	??	*	*	UNID		Y
RX J1739.4-2942	X	0.16	17	39	30.30	-29	42	8.9	A	*	*	Be/X	Be	Y
RX J1740.7-2818	X	*	*	*	*	*	*	*	??	*	*	UNID		Y
RX J1741.4+0348	X	0.67	17	41	28.26	3	48	52.9	PMM0900-10385820	*	15.30	AGN	Sy 1	
RX J1742.3-2737	X	*	*	*	*	*	*	*	??	*	*	UNID		Y
RX J1749.8-3312	X	*	*	*	*	*	*	*	SLX 1746-331	*	*	UNID		Y
RX J1804.1+0042	X	*	18	4	9.01	0	42	22.1	PMM0900-11515260	*	18.60	Gal		
RX J1925.0+4429	A	0.34	19	25	1.98	44	29	50.2	GSC0314600035	9.71	*	AC	K1V	
RX J1929.8+4622	A	0.38	19	29	50.49	46	22	23.6	PMM1350-10836797	*	17.00	AGN	Sy 1	

Continued on next page

Source Name	Sel	d(x-o) (r <sub>90</sub> )	Right Asce.			Dec			Optical Identification	V	B	Class	Type	Finding Chart
			h	m	s	d	'	"						
RX J1931.1+0937	X	0.39	19	31	9.23	9	37	16.4	A	*	19.00	AGN	Bl Lac	Y
RX J1935.4+3746	A	0.02	19	35	29.40	37	46	9.9	GSC0313500052	11.41	*	AC	M4Ve	
RX J1936.3+2632	S	0.53	19	36	18.73	26	32	56.5	A	*	*	WD	DA	Y
RX J1943.9+2118	X	*	*	*	*	*	*	*	??	*	*	UNID		Y
RX J1946.2-0444	A	0.37	19	46	16.42	-4	44	55.4	PMM0825-16960702	*	19.00	CV		Y
RX J1947.3+3045	S	0.66	19	47	24.38	30	45	55.2	PMM1200-13387458	*	17.10	WD	DA	
RX J1950.0+3821	A	*	*	*	*	*	*	*	??	*	*	UNID		Y
RX J1951.7+3716	A	0.65	19	51	47.53	37	16	48.3	PMM1200-13720959	*	15.50	CV		Y
RX J1953.6+5025	B	0.30	19	53	40.76	50	24	57.2	PMM1350-11463233	*	15.80	AC	M3Ve	
RX J1956.7+5304	B	0.30	19	56	46.11	53	4	23.2	GSC0393501634	10.34	*	AC	K0V	
RX J2002.1+5438	B	0.61	20	2	7.40	54	37	47.0	HD 190398	8.20	9.40	AC	G0V	
RX J2010.5+0632	B	0.50	20	10	34.41	6	32	17.4	GSC0050701588	12.01	*	AC	Me	
RX J2014.8+4501	B	0.72	20	14	49.04	45	1	46.4	HD 192785	9.20	10.30	AC	K0V	
RX J2019.8+2256	A	0.79	20	19	49.23	22	56	35.1	GSC0215501614	11.40	*	AC	M4Ve	
RX J2021.7+5213	A	0.63	20	21	44.59	52	13	38.6	GSC0358400565	11.84	*	AC	G3V	
RX J2033.4+3128	B	0.73	20	33	24.41	31	28	12.6	GSC0268600876	10.35	*	AC	G7V	
RX J2040.3+1059	B	0.24	20	40	18.55	10	59	45.2	PMM0975-19711620	*	16.10	AGN	Sy 1	
RX J2043.9+5314	X	0.26	20	43	59.60	53	14	34.9	PMM1425-11257915	*	17.50	AGN	Sy 1	
RX J2044.0+2833	B	0.52	20	44	4.50	28	33	12.1	PMM1125-17121513	*	14.70	AGN	Sy 1	
RX J2102.0+3359	S	*	*	*	*	*	*	*	?? UV excess object	*	*	UNID		Y
RX J2102.6+4553	A	0.84	21	2	38.67	45	52	58.4	HD 200560	7.68	8.65	AC	K3V	
RX J2104.2+2118	X	*	*	*	*	*	*	*	??	*	*	UNID		Y
RX J2109.7+4029	X	0.87	21	9	48.50	40	29	23.9	GSC0317201505	10.70	*	AC	G2V	
RX J2133.7+5107	B	0.21	21	33	43.64	51	7	24.4	PMM1350-14702073	*	15.80	CV		Y
RX J2155.3+5938	S	0.69	21	55	23.70	59	38	36.6	PMM1425-12649991	*	12.70	AC	M4Ve	
RX J2156.3+3318	B	0.24	21	56	23.04	33	18	35.9	PMM1200-18997159	*	16.20	Gal		
RX J2255.0+5540	X	0.44	22	55	4.57	55	40	52.5	GSC0398901784	9.42	*	AC	G0V	
RX J2322.6+6113	X	0.38	23	22	40.08	61	13	33.5	GSC0427901821	9.79	*	AC	G0V	